MS—RAND—GMR—Product
2005/06)

Validation of the tropospheric chemistry component of UKCA

Fiona M. O'Connor*, Colin E. Johnson*, and Olaf Morgenstern†
*Hadley Centre and †University of Cambridge

Contract deliverable reference number: I.1

File: M/GMR/6/3 Annex A

Revision History by Authors

Author	Revision date	Summary of changes
Fiona O'Connor	03/05/2006	Started draft
Fiona O'Connor	08/05/2006	Draft completed

Approvals

This document requires the following approvals from the relevant activity manager and/or lead scientist and contract manager:

Name	Title	Date of Issue	Version
Derrick Ryall	Hd(GMR)	date	1

1 Introduction

The overall aim of the Atmospheric Composition Project is to improve our capability of modelling the Earth's climate system, in which chemistry and aerosols are key components. By developing and improving the way in which chemistry and aerosols are represented in the climate system, our ability to model the Earth's response to perturbations will be improved. This aim will be addressed by the developments proposed in the UKCA project. The United Kingdom Chemistry and Aerosols (UKCA) project is a joint Met Office-NCAS (NERC Centres for Atmospheric Science) initiative to develop a tropospheric and stratospheric chemistry and aerosols model which will be implemented in the Hadley Centre's climate model, HadGEM1. It will include a number of chemical schemes with varying degrees of complexity appropriate for tropospheric, stratospheric, and/or troposphere-stratosphere studies. The aerosol component of UKCA will include dynamically varying aerosol size distributions, internally mixed aerosols, and new aerosol types such as sea salt and ammonium nitrate. The scope of UKCA is wide-ranging, however, this report will only focus on the evaluation of the UKCA tropospheric chemistry model in HadGEM1.

The UKCA model makes use of the Unified Model's online tracers and transport schemes for large-scale and convective transport and boundary layer mixing. As a result, the first part of the report will concentrate on the evaluation of the UM's transport scheme by using simple tracers such as radon and krypton. In addition, wet scavenging by the UM's large-scale and convective precipitation will be assessed through the use of another idealised tracer, lead. Finally, the report will focus on the evaluation of the tropospheric chemistry within UKCA against climatological surface observations and vertical profiles. Where possible, comparisons with STOCHEM, the Met Office's existing tropospheric chemistry model, will also be included.

2 Tracer Experiments

2.1 Radon

Radon has long been recognised as a useful tracer to assess a global model's convective and synoptic-scale motions (e.g. Brost and Chatfield 1989) because of its simple source and sink terms. It is emitted from all non-frozen land at a global emission rate of 15 kg/year. This simple emissions scenario is the same as that used in the World Climate Research Program (WCRP) global model intercomparison (Jacob *et al.* 1997) and is considered to be accurate to within 25 % globally (Turekian *et al.* 1977). Removal of radon from the atmosphere is by radioactive decay with a half-life of 3.8 days. It is because of its surface source and short lifetime that radon's abundance in the atmosphere is largely determined by convective transport and boundary layer mixing.

Figure 1 shows a comparison of modelled surface concentrations from UKCA and STOCHEM against observations at a number of selected surface sites. Both models are driven by meteorology from HadGEM1 but their transport schemes are different. There are stations (e.g. Dumont Urville) where both models fail to capture the correct elevated surface concentrations during the Northern Hemisphere winter. This was also noted by Josse *et al.* (2004) and was attributed in the MOCAGE model to the representation of sea ice extent in the model and the inability of polar storms to penetrate the Antarctic continent correctly. Equally, there are some sites at which the performance of UKCA is better than STOCHEM (e.g. Cape Grim) and others at which STOCHEM outperforms UKCA (e.g. Bombay). However, the comparison indicates that both models generally capture the seasonal cycle and absolute concentrations of radon at most stations.

In order to evaluate the performance of UKCA quantitatively against STOCHEM and the surface observations, the use of Taylor Diagrams is adopted. These diagrams provide a useful means of summarising a model's performance on a two-dimensional diagram. Basically, the correlation co-efficient, the ratio of the standard deviation of the model with that of the observations, and the root mean square error between the model and the observations can all be represented by a single point on the 2d diagram; full details can be found in Taylor (2001). Figure 2 shows such a diagram, where the coloured points summarise the performance of a model at all stations for each year of the model integration against the same climatological measurements. The correlation co-efficient of each model with the observations is of the order of 0.9, indicating that the spatial and seasonal variations in the surface observations are being reasonably captured by both models. However, the standard deviation of the UKCA modelled surface concentrations is greater than that from STOCHEM and the observations. This can largely be attributed to the comparison at Bombay, where UKCA strongly overestimates the surface concentrations in the October–February time period.

A comparison between UKCA modelled and observed vertical profiles of radon taken during 11 flights over Moffett Field, California (37.4°N, 122.0°W) can be seen in Fig. 3. All modelled profiles capture the strong vertical gradient in the boundary layer. Only the modelled output from June appears to show the classic C-shaped profile evident in the observations. However, this may be attributable to the fact that 7 out of the 11 flights were during June, with only 1 flight in July and 3 flights in August.

2.2 Lead

Lead (^{210}Pb) is the radioactive decay product of radon. It attaches itself to aerosols in the sub-micron size range and is removed from the atmosphere by dry and wet deposition. For dry deposition, the deposition velocities at 1 metre were prescribed as follows: 0.2 cm/s over land and 0.05 cm/s over the ocean (Balkanski *et al.* 1993). For wet deposition, the aerosols to which lead attaches itself are assumed to be very soluble

and no variation in solubility is taken into account. Scavenging by convective and large-scale precipitation is treated as a first-order loss process according to Walton *et al.* (1988). The only differences in the treatment of convective and dynamic scavenging are in the scavenging coefficients (2.4 cm^{-1} for dynamic and 4.7 cm^{-1} for convective precipitation) and the fraction of the gridbox over which the precipitation occurs (1.0 for dynamic and 0.3 for convective precipitation). Wet deposition is the dominant removal process of lead and hence, this tracer provides an ideal means for assessing the wet deposition scheme in UKCA independently of the chemistry.

Figures 4 and 5 show comparisons of modelled surface lead concentrations from UKCA and STOCHEM against observations in the Northern and Southern Hemispheres, respectively. The observations are taken from surface sites involved in the Surface Air Sampling Program (http://www.eml.doe.gov/databases/sasp/), a summary of which can be found in Table 1. There is excellent agreement between both models and the observations in the Northern Hemisphere in terms of the seasonal cycle and the absolute concentrations. One exception is the comparison at Kap Tobin, where UKCA and STOCHEM both fail to capture the observed seasonal cycle. However, this station has a much shorter record of observations than the others which could contribute to the poor comparison (Table 1). In the Southern Hemisphere, there are some stations at which both UKCA and STOCHEM fail to capture the correct seasonal cycle and/or absolute concentrations (e.g. Chacaltay, Chatham Island). However, there are also others where the comparison is excellent (e.g. La Reunion, Cape Grim). Furthermore, there are a number of stations where STOCHEM appears to outperform UKCA (e.g. Falklands, Perth). Although both models are being driven by the same climate model, there are a number of differences which could account for the different performances. The large-scale and convective transport schemes are different. In the case of lead deposition, the scavenging co-efficients and the treatment of deposition by convective precipitation differ between the two models. In order to do a quantitative evaluation of the two models against the surface lead observations, a Taylor diagram is shown in Fig. 6 where each point represents the performance of output from each model year. It shows that the correlation co-efficient of UKCA and STOCHEM are high (0.85 for UKCA and approximately 0.9 for STOCHEM, indicating that both models capture the spatial and seasonal variations in the surface observations very well. As was the case for radon, the standard deviation of the STOCHEM concentrations matches more closely that of the observations than UKCA. As a result, the STOCHEM points lie closer to the "perfect model" position, confirming that the overall performance of STOCHEM is better than UKCA.

In addition to the surface ^{210}Pb concentrations, the 5 years of UKCA model output were used to obtain mean annual deposition fluxes at the surface. These are compared in Fig. 7 with gridded surface flux measurements compiled by Preiss and Genthon (1997). Although there is significant scatter about the 1:1 line, there is still good correlation between UKCA and the observed deposition fluxes (correlation co-efficient

= 0.78). Furthermore, Fig. 8 shows comparisons between vertical profiles of lead from UKCA and observations taken during the PEM West B aircraft campign (Dibb *et al.* 1997) over the "remote Pacific" and "near Asia" regions. It indicates that modelled lead concentrations in the mid and upper troposphere are reasonably well simulated but the model fails to capture the observed concentrations in the lower troposphere. This could be attributed to the fact that UKCA is running in climate mode and its climatology may be different from the meteorological conditions encountered during PEM West B.

2.3 Krypton

Krypton (^{85}Kr) is released from the re-processing of nuclear fuel and is removed from the atmosphere by radioactive decay to rubidium with an e-folding lifetime of 15.52 years. In this experiment, ^{85}Kr was emitted from seven known point sources in the Northern Hemisphere during the period 1978–1983. The strength of these sources was taken from Jacob *et al.* (1987). ^{85}Kr was also emitted from a nuclear re-processing plant in the former USSR, whose strength was estimated by Jacob *et al.* (1987). Its long lifetime and the fact that its sources are solely in the Northern Hemisphere make krypton useful in assessing the inter-hemispheric transport timescale in a global model.

The experiment was initialised on 1 September 1978, with initial ^{85}Kr concentrations taken from Rind and Lerner (1996). Modelled concentrations were verified by comparison with observations taken during nine ship cruises over the Atlantic Ocean between 1980 and 1987 (as reported by Jacob *et al.* 1987). The comparison for March in Fig. 9a clearly shows that there is a strong difference between the model years and that the results for March 1983 will be sensitive to the model initialisation. However, the meridional gradient seems quite robust in all model years and occurs at approximately 0°N. This matches quite well with the observed tropical gradient. The comparison between UKCA and measurements for October (Fig. 9b) shows that there is a good correspondence between modelled and measured concentrations in 1980 except that the tropical gradient in the model is shifted equatorward by about 10° in comparison with the observations. This was also the case in the evaluation of the LMDz model by Hauglustaine *et al.* (2004), and was attributed to a reduced seasonal cycle in the Intertropical Convergence Zone (ITCZ) location. For October 1983, modelled concentrations in the Southern Hemisphere appear too high, the tropical gradient is again shifted equatorward, and the low observed concentrations at 40°N are not well simulated. However, the modelled inter-hemispheric difference in the surface concentrations matches the observed inter-hemispheric difference and as a result, the modelled concentrations can be used to evaluate an inter-hemispheric transport timescale for HadGEM1.

In an idealised two-box model, the inter-hemispheric difference in mean concentration, C_{ns}, evolves with time according to (Jacob *et al.* 1987):

$$\frac{dC_{ns}}{dt} = \frac{E - 1.96C_{ns}(2t_e - 1 + t_d - 1)}{1.96} \tag{1}$$

where $C_{ns} = C_n - C_s$ is the difference between the mean Northern and Southern Hemispheric concentrations (in pCi/m^3 at STP), E is the emission rate (in MCi/year), t_e is the inter-hemispheric transport timescale (in years), and t_d is the e-folding lifetime (in years). If C_{ns} reaches a steady state, then:

$$\frac{dC_{ns}}{dt} = 0 \tag{2}$$

and the inter-hemispheric transport timescale can be computed from the steady state value of C_{ns} as follows:

$$t_e = \left(\frac{E}{3.92C_{ns}} - \frac{1}{2t_d}\right)^{-1} \tag{3}$$

In this experiment, C_{ns} was reasonably stable throughout the integration. Taking an average value of C_{ns} of 2.057 pCi/m^3 at STP, and a mean emission rate for the years 1978–1983 of 6.33 MCi/year, the inter-hemispheric transport timescale was estimated at 1.33 years. This value is larger than the value of 1.1 years estimated by Jacob *et al.* (1987) but close to that estimated from CFC and Krypton experiments in the GISS model by Rind and Lerner (1996).

3 Tropospheric Chemistry

A tropospheric chemistry scheme involving 24 tracers, 27 photolysis reactions and 101 gas-phase reactions has been included in UKCA. The chemistry involves the oxidation of methane, ethane, and propane, with the option of including the Mainz Isoprene Mechanism (Pöschl *et al.* 2000). The model does not yet have a reresentation of heterogenous reactions. However, surface, lightning, and aircraft emissions are included and processes such as dry deposition, convective and large-scale washout are also considered. As this scheme lacks stratospheric CFC chemistry, boundary conditions are required at the top of the model domain. For ozone, methane, and NO_y, all levels above 30 hPa are set to values taken from a climatology derived from the Cambridge two-dimensional model (Law and Pyle 1993).

Figure 10 shows surface carbon monoxide concentrations compared with observations at selected sites. UKCA captures the seasonal cycle at all the surface sites very well. At the Northern Hemisphere sites, the absolute concentrations match the observations reasonably. Modelled concentrations in the Southern Hemisphere are too high (e.g. Cape Grim, Syowa), probably indicating incorrect emissions there. Figure 11 shows the corresponding comparison for surface ozone concentrations. The model simulates the springtime ozone maxima at Northern Hemisphere sites, though this persists

for too long (e.g. Mace Head, Niwot Ridge). The seasonal cycles at Mauna Loa and Bermuda closely match the observations, but the summertime ozone concentrations are too high at Cape Grim. This is possibly because both carbon monoxide and methane concentrations are also too high there.

Given the mixed performance at the various stations in relation to absolute concentrations and seasonal cycle, a quantitative assessment of the surface comparisons is required. For this, a number of statistical measures of skill have been evaluated at each of the surface sites and are shown in Tables 2–4 for carbon monoxide, methane, and ozone. For carbon monoxide, the correlation co-efficient is greater than 0.8 at all stations, confirming that the seasonal cycle is captured very well by UKCA. However, the model skill score and the absolute and relative annual mean biases confirm that in the Southern Hemisphere mid and high latitudes, absolute concentrations are too high by at least 30%. For methane, the modelled seasonal cycle is good at all stations (correlation co-efficients are all positive and greater than 0.6) and the absolute and relative mean biases are excellent. For ozone, the statistical measures of skill are quire varied, indicating that the performance of UKCA at the various stations is mixed. The correlation co-efficients confirm that at some stations (e.g. Barrow, Barbados), the modelled seasonal cycle is poor whereas at others (e.g. Bermuda, Mauna Loa), UKCA captures the seasonal cycle very well. The model scores and absolute and relative annual mean biases show that at some stations (e.g Mauna Loa, Bermuda), modelled concentrations match closely with observations but at others, UKCA performs poorly. Finally, the overall performance of the tropospheric chemistry for each model year relative to the surface observations is summarised in a Taylor diagram, shown in Fig. 12. It indicates that there is significant interannual variability in carbon monoxide. A look at Fig. 10 will indicate that this is largely due to the variability of modelled concentrations at Mace Head during Spring. The Taylor diagram also confirms that the performance of UKCA is better for carbon monoxide and methane than for ozone.

A comparison between modelled and measured ozone profiles for a selection of sites can be seen in Figs. 13 and 14 for January and July, respectively. Although only a small number of sites are shown, the observational dataset is that from Logan (1999) and encompasses about 40 sites worldwide. The figures indicate that UKCA is capable of capturing the vertical gradient of ozone and its absolute concentration throughout the vertical domain of the model at these selected sites. At some locations, the comparison between UKCA and the observed climatology is remarkable (e.g. Kagoshima in January and July). However, there are also some locations (e.g. Alert) where the performance of UKCA is less favourable. The annual cycle of modelled and measured ozone concentrations are compared at various stations on a number of pressure levels (1000, 900, 700, 500, 300, 200, 100, and 30 hPa). The comparisons for 700 and 300 hPa are shown in Fig. 15 and the corresponding scatter plots can be seen in Fig. 16. They indicate that overall, modelled ozone at 700 hPa compares very well with the climatology from Logan (1999). However, at 300 hPa, modelled ozone is systematically too high.

Some reduction in modelled ozone in the lower stratosphere is obtained by updating reaction rate co-efficients to 2005 recommendations (not shown). In addition, at some Northern high-latitude stations, the modelled tropopause is below 300 hPa whereas the climatology suggests that the tropopause should be higher. This can account for some of the bias in Figs. 15 and 16b. Finally, a Taylor diagram summarising the comparison between modelled ozone from UKCA and measured ozone at all the pressure levels considered can be seen in Fig. 17. It indicates that the UKCA model performs well in the lower to mid-troposphere. However, the performance is not so good in the lower stratosphere. This cannot be attributed to poor boundary conditions prescribed at the upper boundary as the comparison at 30 hPa is very good.

4 Conclusions

The development of UKCA is progressing well and this report highlights some of the first results from the model. Because the UM's transport scheme forms the basis of UKCA, the first part focussed on an assessment of the tracer transport scheme. Using idealised tracers such as radon, lead, and krypton, convective transport and boundary layer mixing, wet deposition, and inter-hemispheric transport were evaluated independently of the chemistry. Results from a tropospheric chemistry scheme successfully implemented in UKCA were presented and evaluated using climatological measurements of ozone, methane, and carbon monoxide.

Further work on UKCA tropospheric chemistry is planned and/or already underway. This includes the optimisation and porting of the Fast-J photolysis scheme (Wild *et al.* 2000) as an on-line component, sulphur chemistry, interactive dry deposition, and heterogeneous chemistry.

5 References

Balkanski, Y. J., D. J. Jacob, and G. M. Gardner, Transport and residence times of tropospheric aerosols inferred from a global three-dimensional simulation of ^{210}Pb, *J. Geophys. Res.*, 98, 29573–20586, 1993.

Brost, R. A. and R. B. Chatfield, Transport of radon in a three-dimensional, subhemispheric model, *J. Geophys. Res.*, 94, 5095–5119, 1989.

CMDL - Climate Monitoring and Diagnostics Laboratory (now Global Monitoring Division of Earth System Research Laboratory): http://www.cmdl.noaa.gov, 2005.

Dibb, J. E., R. W. Talbot, B. L. Lefer, E. Scheuer, G. L. Gregory, E. V. Browell, J. D. Bradshaw, S. T. Sandholm, and H. B. Singh, Distributions of beryllium 7 and lead 210, and soluble aerosol-associated ionic species over the western Pacific: PEM West B, February–March 1994, *J. Geophys. Res.*, 102, 28287–28302, 1997.

Hauglustaine, D. A., F. Hourdin, L. Jourdain, M. A. Filiberti, S. Walters, J. F. Lamarque, and E. A. Holland, Interactive chemistry in the Laboratoire de Météorologie Dynamique general circulation model: Description and background tropospheric chemistry evaluation, *J. Geophys. Res.*, 109, D04314, doi:10.1029/2003JD003957, 2004.

Jacob, D.J., M. J. Prather, S. C. Wofsy, and M. B. McElroy, Atmospheric distribution of ^{85}Kr simulated with a general circulation model, *J. Geophys. Res.*, 92, 6614–6626, 1987.

Jacob, D. J., M. J. Prather, P. J. Rasch, R.-L. Shia, Y. J. Balkanski, S. R. Beagley, D. J. Bergmann, W. T. Blackshear, M. Brown, M. Chiba, M. P. Chipperfield, J. deGrandpré, J. E. Dignon, J. Feichter, C. Genthon, W. L. Grose, P. S. Kasibhatla, I. Köhler, M. A. Kritz, K. Law, J. E. Penner, M. Ramonet, C. E. Reeves, D. A. Rotman, D. Z. Stockwell, P. F. J. vanVelthoven, G. Verver, O. Wild, H. Yang, and P. Zimmermann, Evalution and intercomparison of global atmospheric transport models using ^{222}Rn and other short-lived tracers, *J. Geophys. Res.*, 102, 5953–5970, 1997.

Josse, B., P. Simon, and V.-H. Peuch, Radon global simulation with the multiscale chemistry and transport model MOCAGE, *Tellus*, 56B, 339–356, 2004.

Kritz, M. A., S. W. Rosner, and D. Z. Stockwell, Validation of an off-line three-dimensional chemical transport model using observed radon profiles - 1. Observations , *J. Geophys. Res.*, 103, 8425–8432, 1998.

Law, K. S. and J. A. Pyle, Modeling trace gas budgets in the troposphere .1. ozone and odd nitrogen, *J. Geophys. Res., 98, 18377–18400, 1993.*

Logan, J. A., An analysis of ozonesonde data for the troposphere: Recommendations for testing 3-D models and development of a gridded climatology for tropospheric ozone, *J. Geophys. Res.*, 104, 16115–16149, 1999.

Oltmans, S. J., H. Levy II, Surface ozone measurements from a global network, *Atmos. Environ.*, 28, 9–24, 1994.

Pöschl, U., R. vonKuhlmann, N. Poisson, and P. J. Crutzen Development and intercomparison of condensed isoprene oxidation mechanisms for global atmospheric modeling, *J. Atmos. Chem.*, 37, 29–52, 2000.

Preiss, N., and C. Genthon, Use of a new database of lead-210 for global aerosol model validation, *J. Geophys. Res.*, 102, 25347–25357, 1997.

Rind, D. and J. Lerner, Use of on-line tracers as a diagnostic tool in general circulation model development 1. Horizontal and vertical transport in the troposphere, *J. Geophys. Res.*, 101, 12667–12683, 1996.

Taylor, K. E., Summarizing multiple aspects of model performance in a single diagram, *J. Geophys. Res.*, 106, 7183–7192, 2001.

Turekian, K. K., Y. Nozaki, and L. K. Benninger, Geochemistry of atmospheric radon and radon products, *Annu. Rev. Earth Planet. Sci.*, 5, 227–255, 1977.

Walton, J. J., M. C. MacCracken, and S. J. Ghan, A global-scale lagrangian trace species model of transport, transformation, and removal processes, *J. Geophys. Res.*, 93, 8339–8354, 1988.

Wild, O., X. Zhu, and M. J. Prather, Fast-j: Accurate simulation of in- and below-cloud photolysis in tropospheric chemical models, *J. Atmos. Chem.,* 37, 245–282, 2000.

6 Tables

Location	Latitude (°N)	Longitude (°E)	No. of monthly mean observations	Years
Thule	77	293	155	1960-1999
Barrow	71	204	196	1975-1999
Kap Tobin	70	338	26	1974-1976
Moosonee	51	280	250	1957-1999
Beaverton	46	237	154	1986-1999
Rexburg	44	293	137	1986-1999
Chester	41	249	120	1987-1998
Montgomery	32	274	87	1989-1999
Miami	26	280	137	1957-1994
Mauna Loa	19	204	250	1957-1999
Guayaquil	-2	280	175	1960-1999
Chacaltaya	-16	292	251	1957-1999
La Reunion	-21	56	85	1990-1999
Norfolk Is.	-29	168	189	1983-1999
Perth	-32	116	190	1982-1999
Cape Grim	-40	144	165	1987-1998
Chatham Is.	-44	184	152	1983-1996
Invercargill	-46	168	186	1983-1999
Falklands	-51	302	129	1987-1999
South Pole	-90	0	195	1974-1999

Table 1: Summary of surface lead observations from the Surface Air Sampling Program (http://www.eml.doe.gov/databases/sasp/).

Station	Latitude °N	Longitude °E	Model Score %	AAMB ppbv	RAMB %	Correlation co-efficient
Barrow	71	-157	100.00	-4.65	-3.30	0.97
Mace Head	53	-10	33.33	32.22	24.23	0.94
Niwot Ridge	40	-106	50.00	28.84	23.29	0.86
Bermuda	32	-64	100.00	9.13	7.17	0.98
Mauna Loa	20	-156	41.67	20.62	21.53	0.97
Barbados	13	-59	66.67	16.48	17.30	0.95
Samoa	-14	-171	58.33	12.23	20.49	0.82
Cape Grim	-41	-145	0.00	28.26	55.57	0.95
Syowa	-69	39	0.00	16.52	33.94	0.99
South Pole	-90	0	0.00	16.98	35.47	0.96

Table 2: Summary of statistical skill scores for the surface carbon monoxide comparison. The model skill score is the percentage of months that the modelled monthly mean concentration of carbon monoxide is within 20% of the observed concentration. The absolute annual mean bias (AAMB) is the difference between the modelled and measured annual mean concentrations while the relative annual mean bias (RAMB) is the AAMB divided by the observed annual mean expressed as a percentage.

Station	Latitude °N	Longitude °E	Model Score %	AAMB ppbv	RAMB %	Correlation co-efficient
Barrow	71	-157	0.00	211.81	11.76	0.87
Mace Head	53	-10	58.33	180.13	9.97	0.69
Niwot Ridge	40	-106	8.33	187.96	10.73	0.64
Bermuda	32	-64	100.00	156.88	8.80	0.86
Mauna Loa	20	-156	25.00	179.29	10.43	0.68
Barbados	13	-59	100.00	147.45	8.46	0.62
Samoa	-14	-171	66.67	157.94	9.49	0.61
Cape Grim	-41	-145	75.00	156.12	9.39	0.94
Syowa	-69	39	100.00	131.12	7.83	0.93
South Pole	-90	0	83.33	149.41	9.03	0.95

Table 3: Summary of statistical skill scores for the surface methane comparison. Here, the model skill score is the percentage of months that the modelled monthly mean concentration of methane is within 10% of the observed concentration.

Station	Latitude °N	Longitude °E	Model Score %	AAMB ppbv	RAMB %	Correlation co-efficient
Barrow	71	-157	33.33	-5.37	-20.70	-0.56
Mace Head	53	-10	58.33	6.69	19.06	0.89
Niwot Ridge	40	-106	83.33	2.74	6.05	0.73
Bermuda	32	-64	75.00	2.60	7.19	0.95
Mauna Loa	20	-156	91.67	0.03	0.07	0.90
Barbados	13	-59	58.33	-1.66	-6.44	-0.21
Samoa	-14	-171	16.67	3.34	24.82	0.89
Cape Grim	-41	-145	58.33	2.94	11.75	0.65
Syowa	-69	39	50.00	-6.71	-24.96	0.22
South Pole	-90	0	41.67	-1.92	-6.60	-0.10

Table 4: Summary of statistical skill scores for the surface ozone comparison. The model skill score is the percentage of months that the modelled monthly mean concentration of ozone is within 20% of the observed concentration. The absolute annual mean bias (AAMB) is the difference between the modelled and measured annual mean concentrations while the relative annual mean bias (RAMB) is the AAMB divided by the observed annual mean expressed as a percentage.

7 Figures

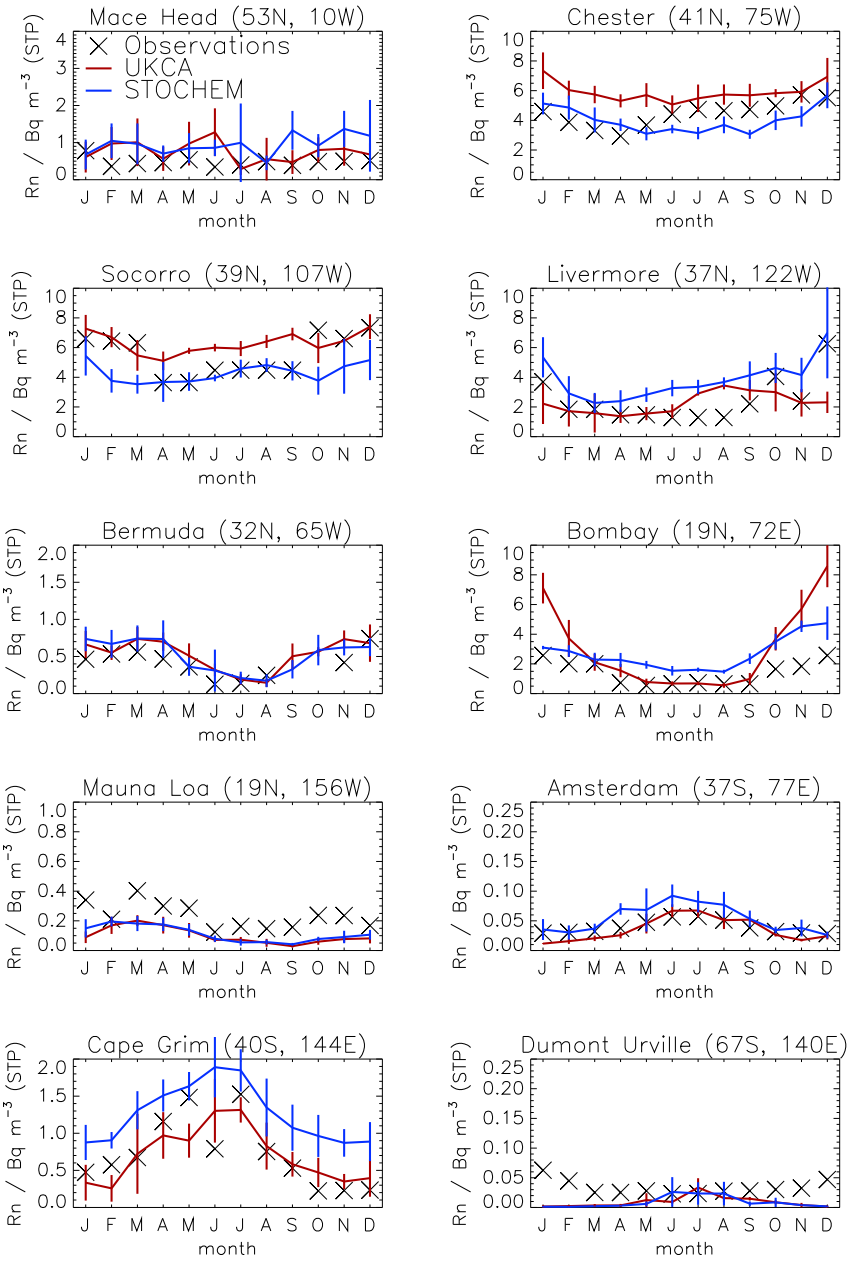

Figure 1: Comparison of modelled surface radon concentrations from UKCA (red) and STOCHEM (blue) with climatological observations (black) as reported by Hauglustaine *et al.* (2004).

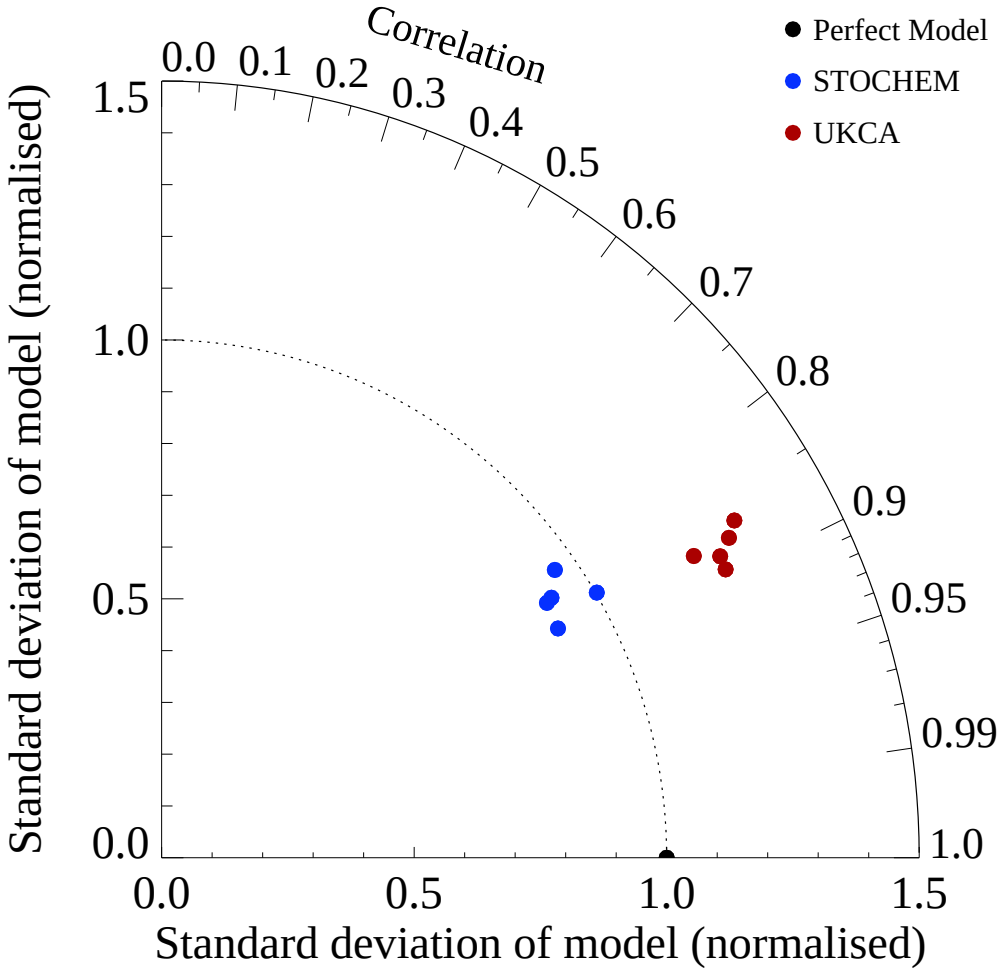

Figure 2: Taylor Diagram indicating the performance of each model year from UKCA (red) and STOCHEM (blue) against the climatological surface ^{222}Rn observations plotted in Fig. 1. The 'perfect model' is represented in black.

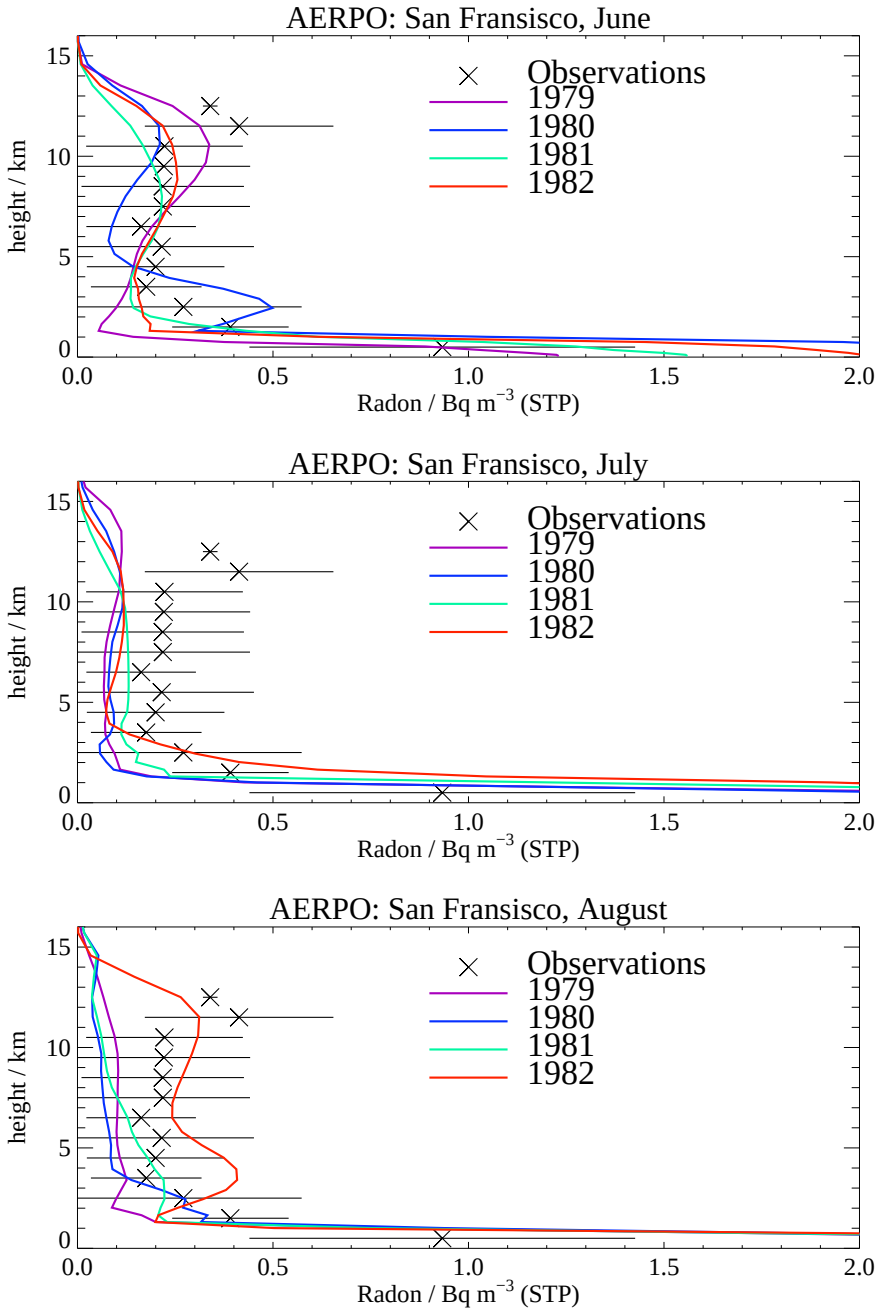

Figure 3: Comparison between modelled and measured vertical profiles of radon over Moffett Field, California (37.4°N, 122.0°W). Measurements taken from Kritz *et al.* (1998).

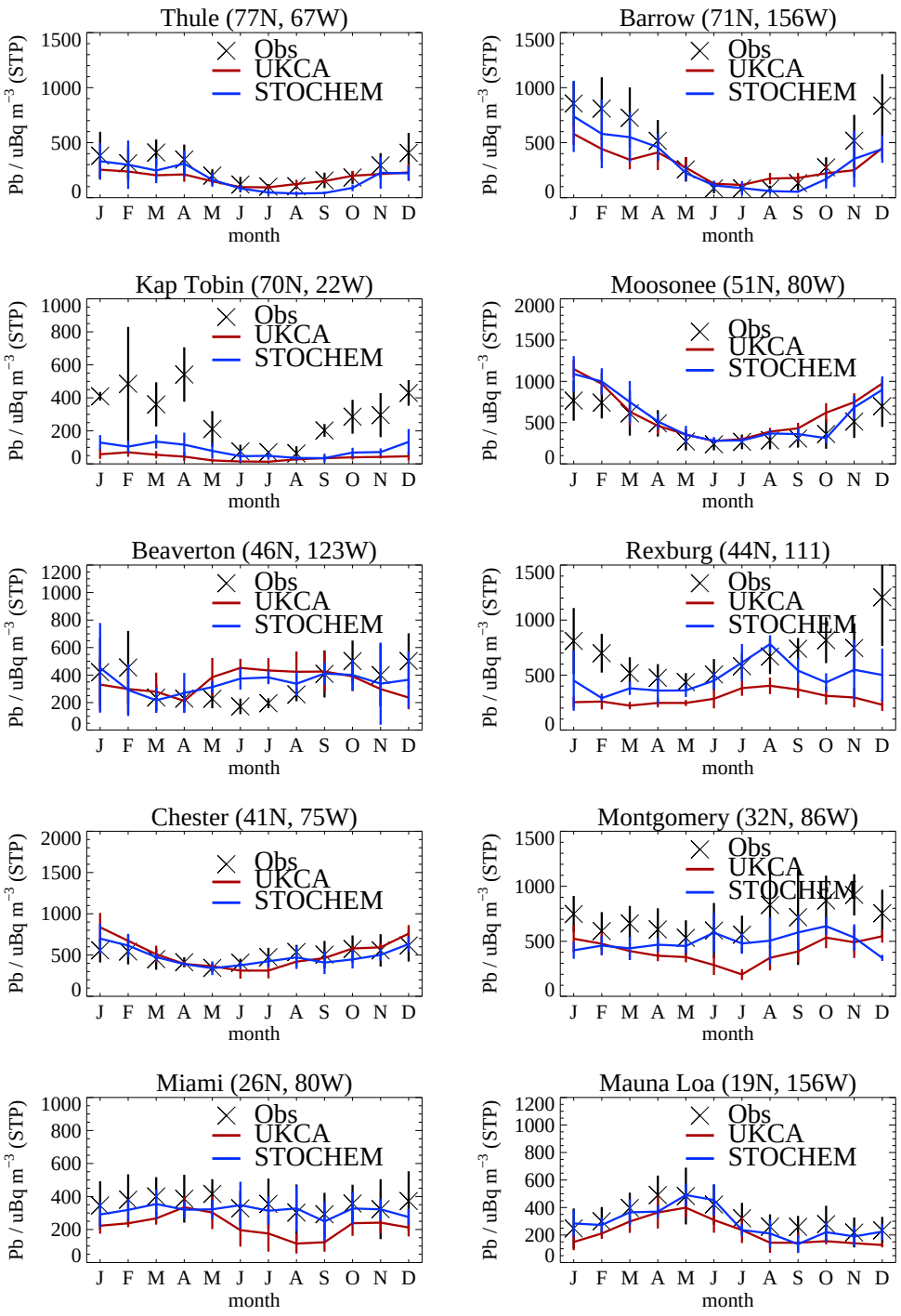

Figure 4: Comparison between modelled lead concentrations from UKCA (red) and STOCHEM (blue) with surface observations from several sites in the Northern Hemisphere. Data are taken from the Surface Air Sampling Program (http://www.eml.doe.gov/databases/sasp/) and are summarised in Table 1.

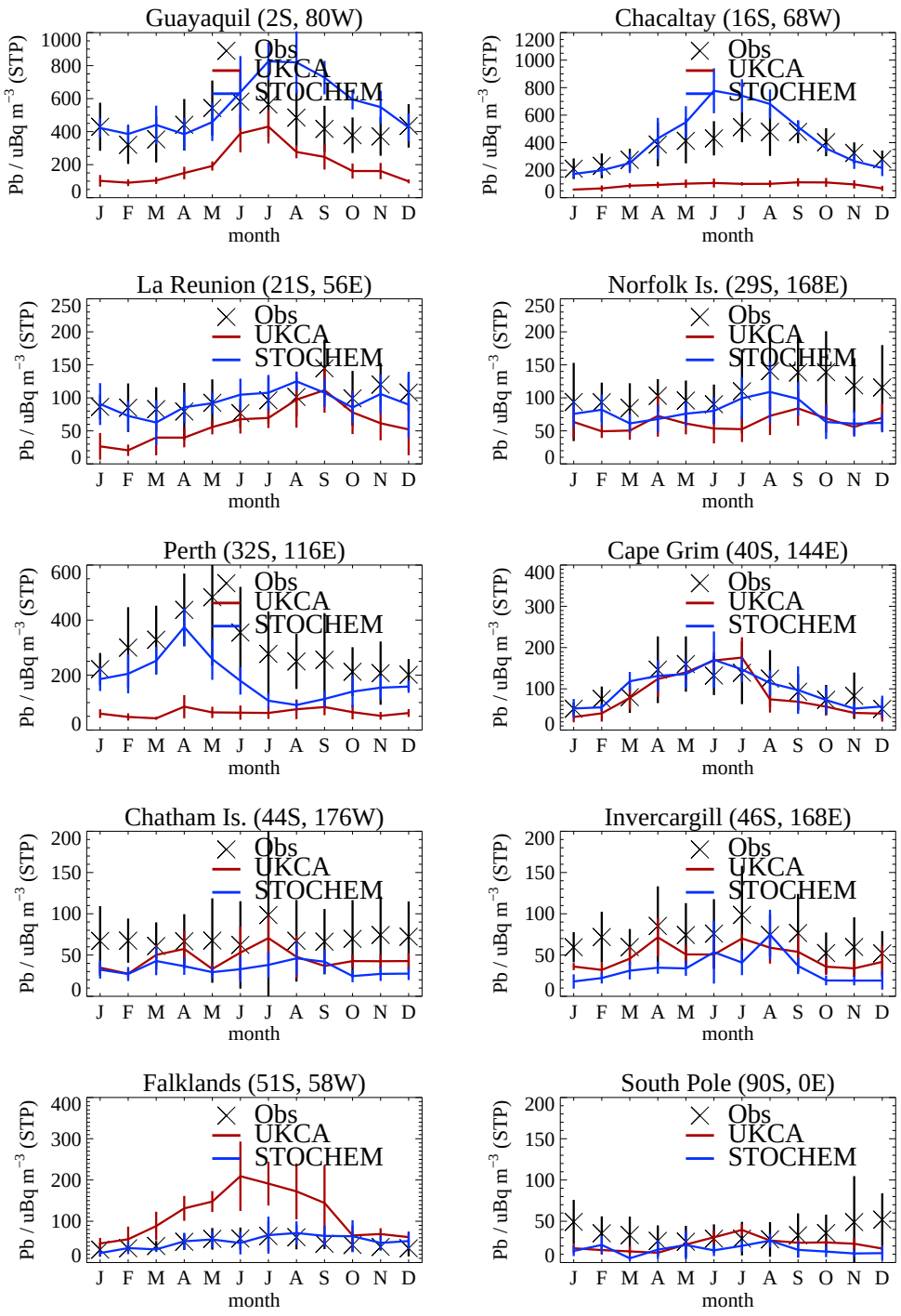

Figure 5: Comparison between modelled lead concentrations from UKCA (red) and STOCHEM (blue) with surface observations from several sites in the Southern Hemisphere. Data are taken from the Surface Air Sampling Program (http://www.eml.doe.gov/databases/sasp/) and are summarised in Table 1.

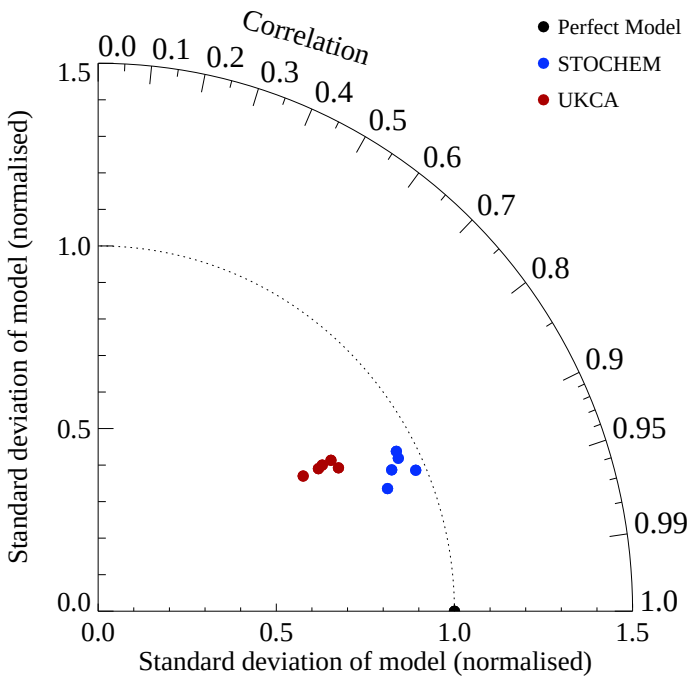

Figure 6: Taylor Diagram indicating the performance of each model year from UKCA (red) and STOCHEM (blue) against the climatological surface observations plotted in Figs. 4 and 5. The 'perfect model' is represented in black.

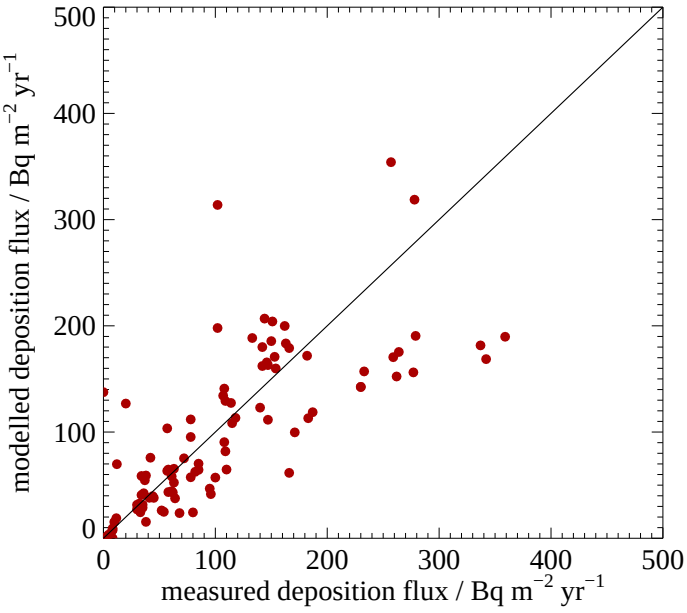

Figure 7: Scatter plot of UKCA annual surface ^{210}Pb deposition fluxes against observed fluxes. Measurements taken from Preiss and Genthon (1997).

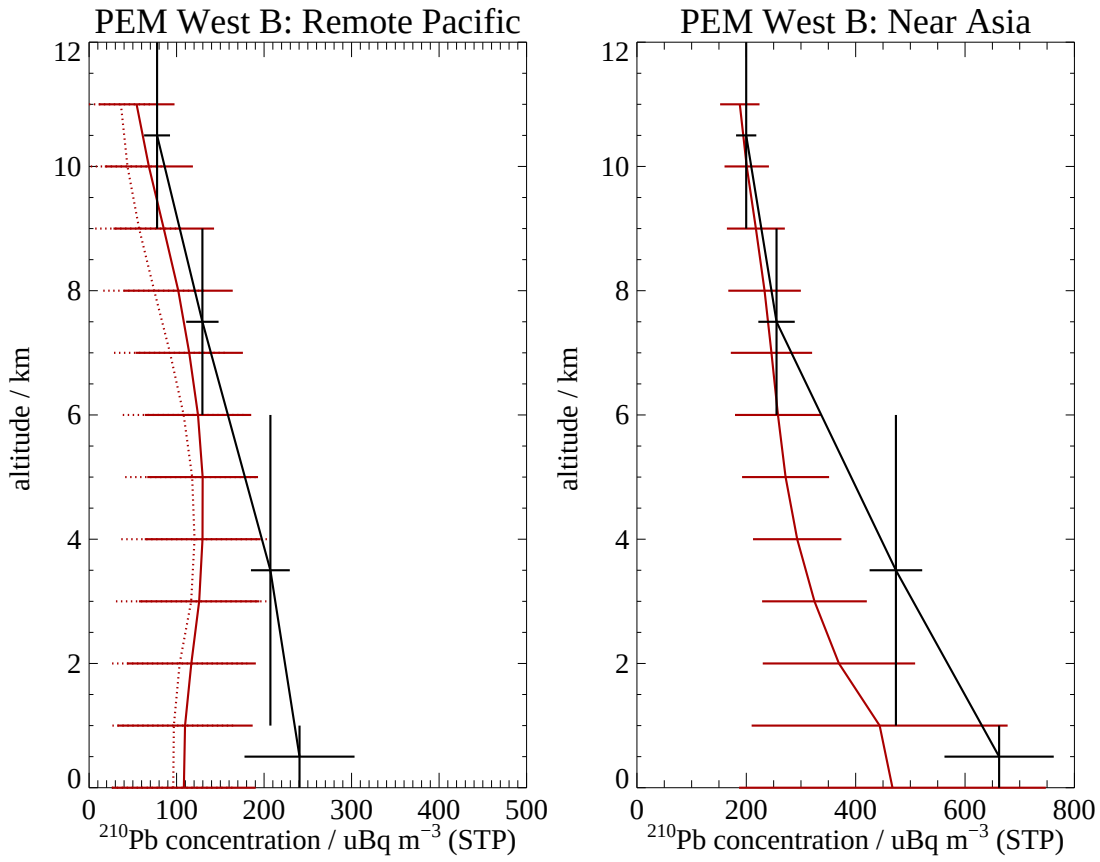

Figure 8: Comparison between vertical profiles of UKCA ^{210}Pb concentrations with observed profiles over the "remote Pacific" and "near Asia" regions sampled during PEM West B. Measurements taken from Dibb *et al.* 1997.

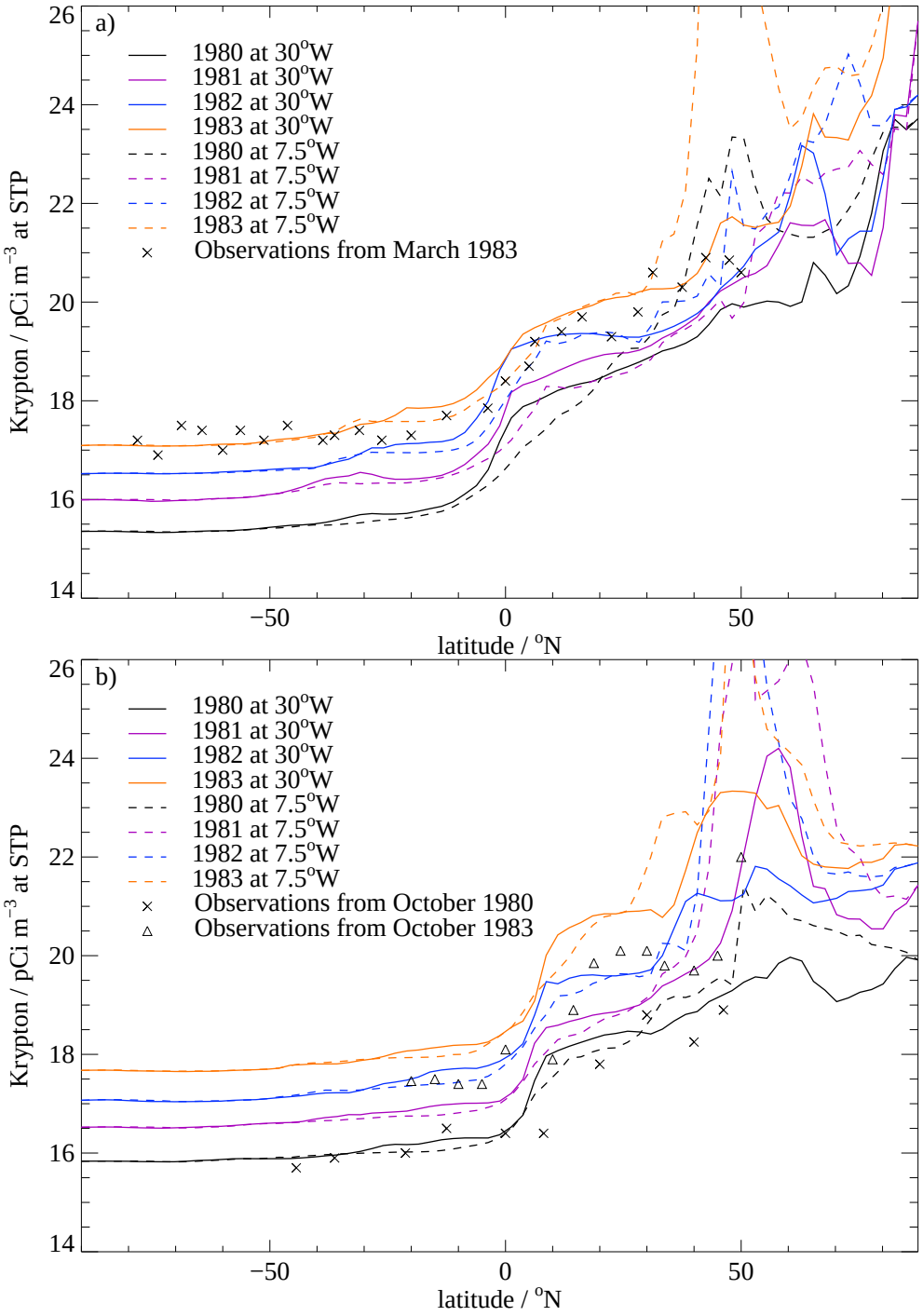

Figure 9: Comparison between modelled and measured surface krypton concentrations over the Atlantic Ocean in a) March and b) October. The observations are those reported by Jacob *et al.* (1987).

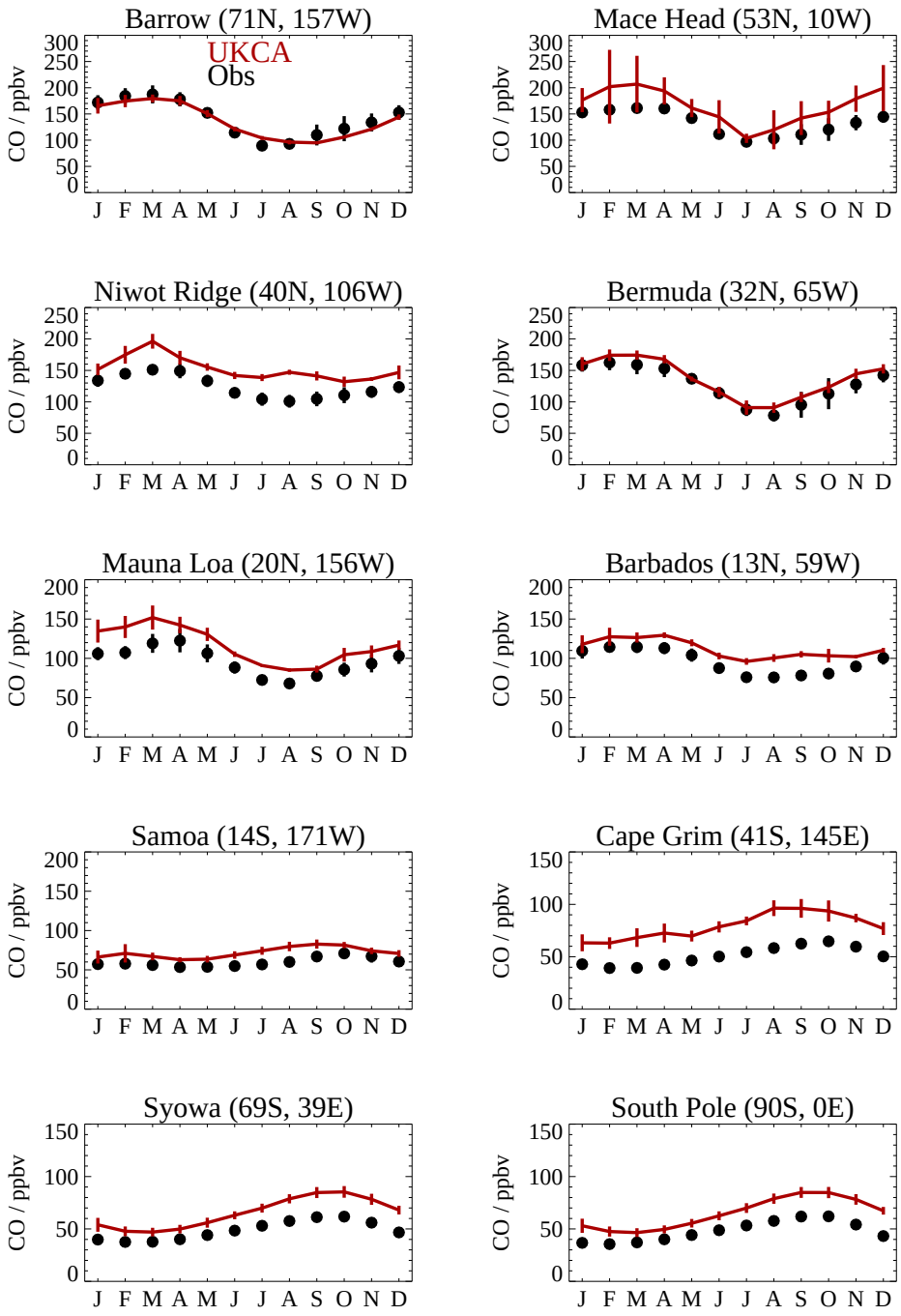

Figure 10: Comparison between modelled (red) and observed (black) surface carbon monoxide concentrations for selected sites. The modelled concentrations are averaged from a 5-year integration. Observations are taken from the CMDL network (CMDL 2005).

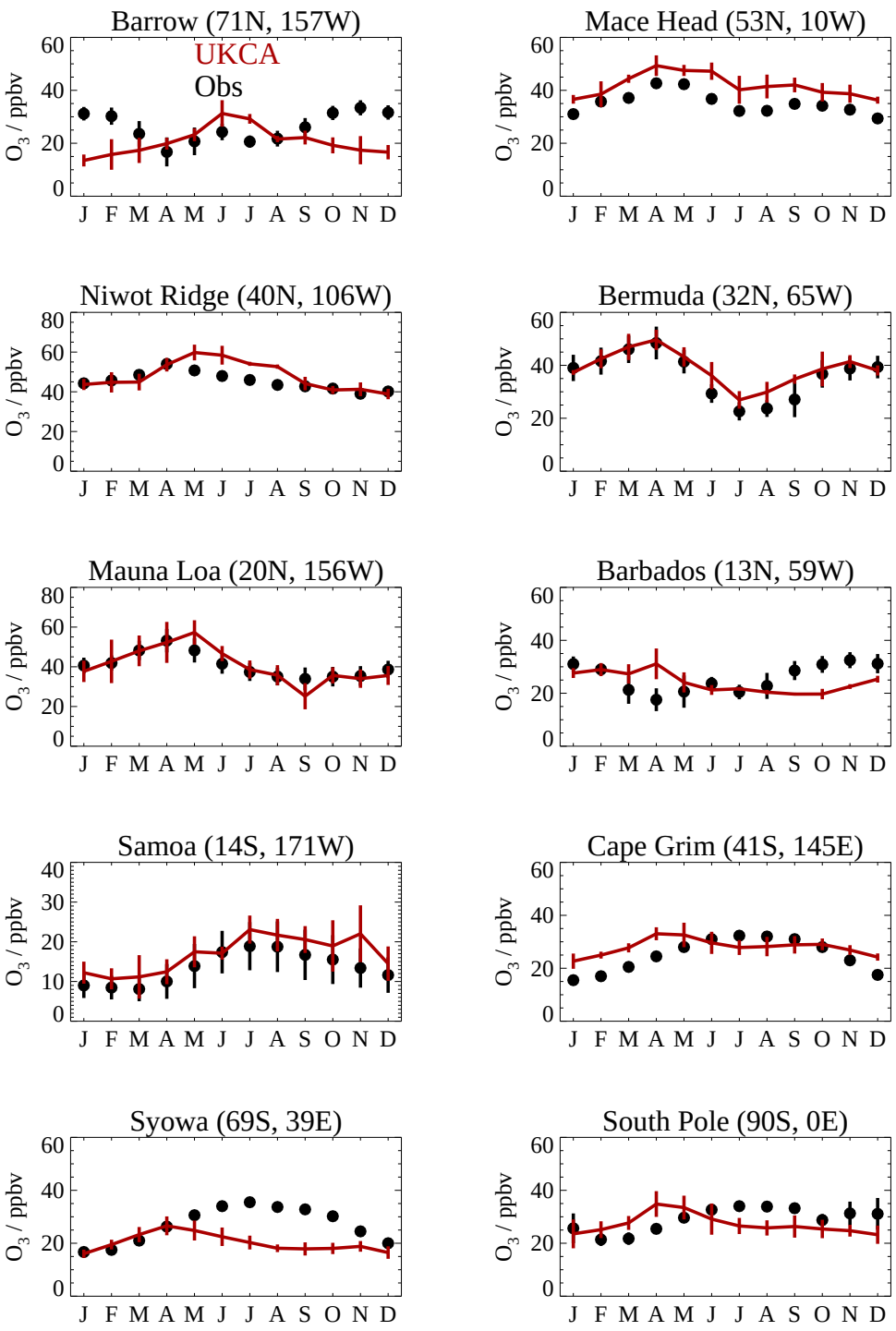

Figure 11: Comparison between modelled (red) and observed (black) surface ozone concentrations for selected sites. The modelled concentrations are averaged from a 5-year integration. Observations are taken from Oltmans and Levy (1994) and the CMDL network (CMDL 2005).

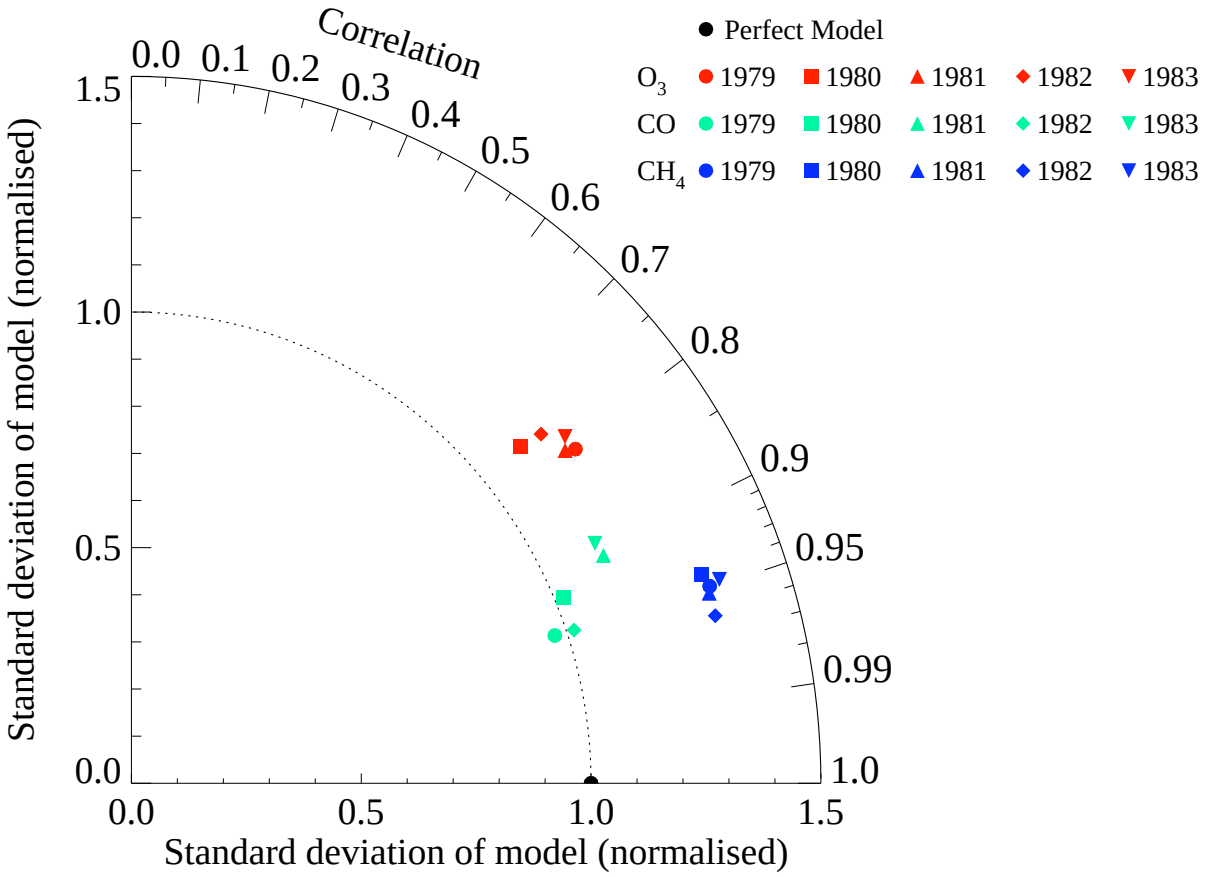

Figure 12: Taylor Diagram indicating the performance of each model year from UKCA for carbon monoxide (green), methane (blue) and ozone (red) against climatological surface observations from Oltmans and Levy (1994) and the CMDL network (CMDL 2005). The 'perfect model' is represented in black.

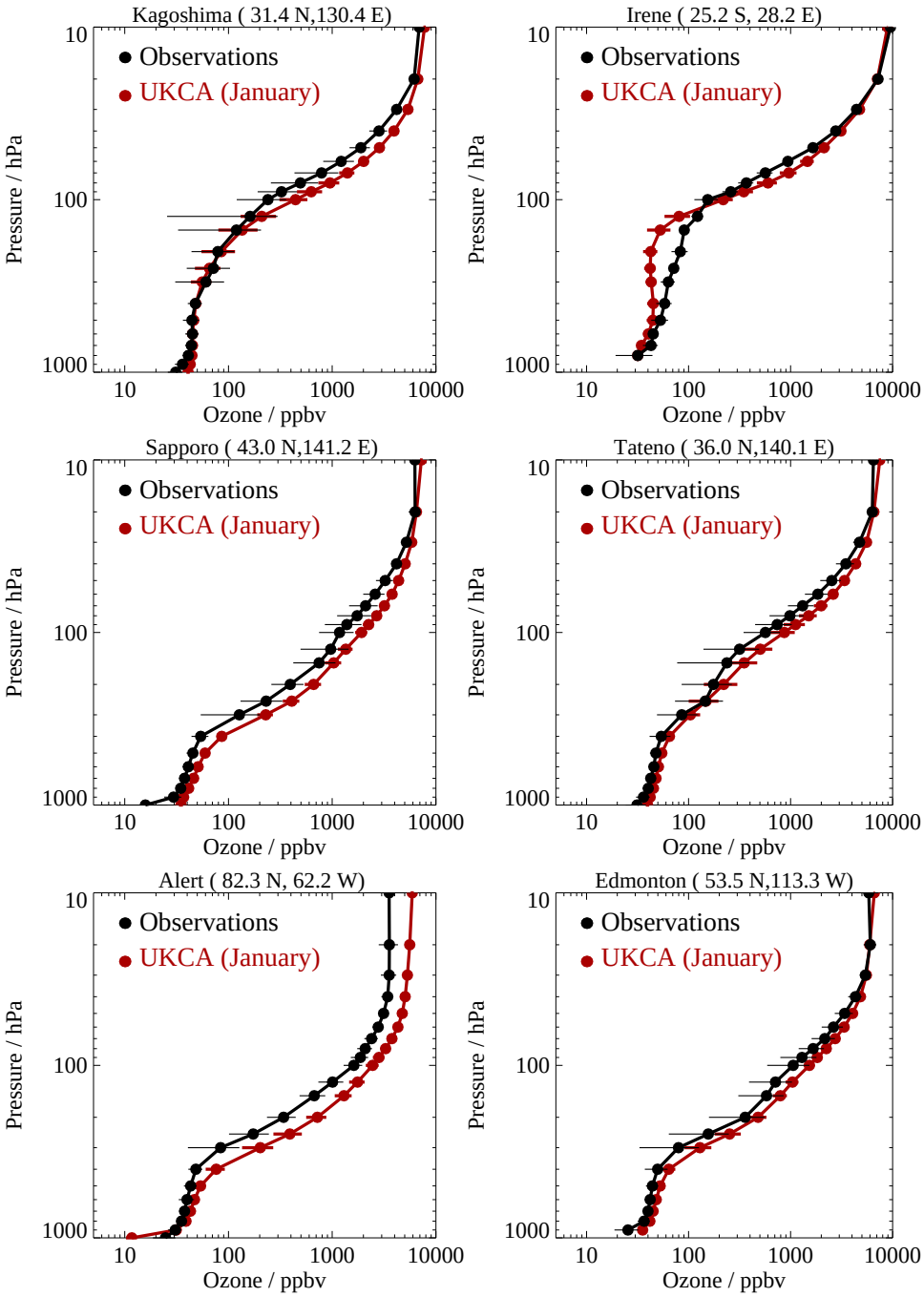

Figure 13: Comparison between modelled (red) and measured (black) vertical profiles of ozone at selected sites in January. The UKCA profiles are averaged from a 5-year model run. The observations are from an analysis by Logan (1999).

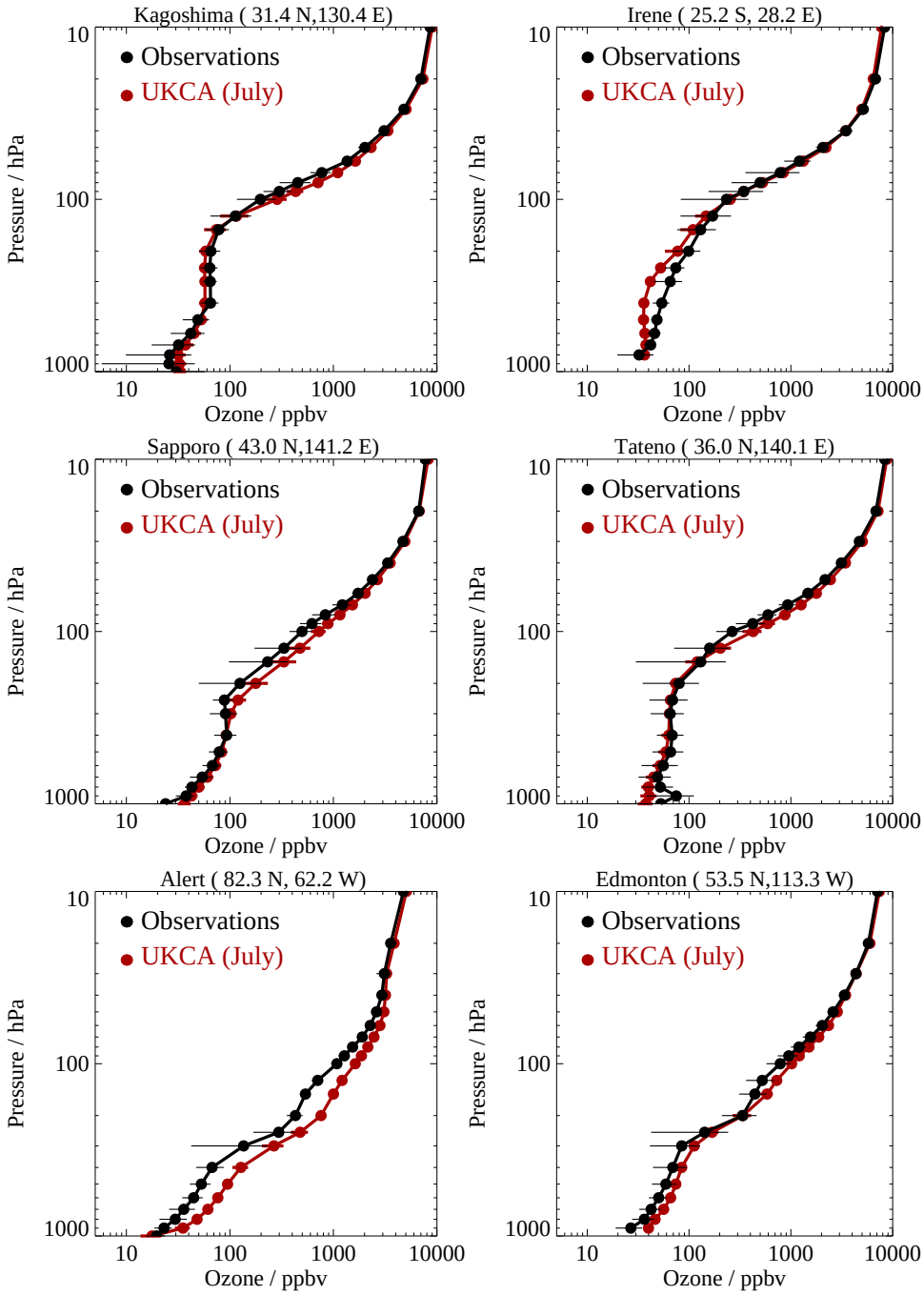

Figure 14: Comparison between modelled (red) and measured (black) vertical profiles of ozone at selected sites in July. The UKCA profiles are averaged from a 5-year model run. The observations are from an analysis by Logan (1999).

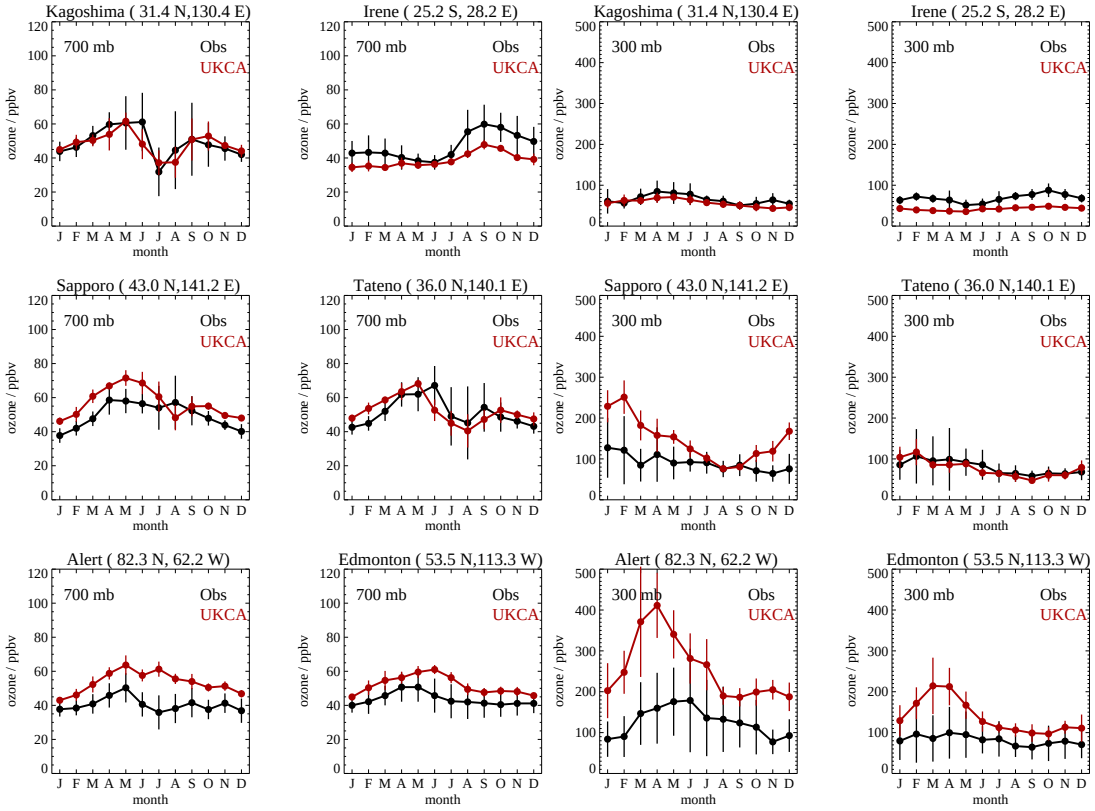

Figure 15: Comparison between modelled (red) and measured (black) ozone concentrations at a) 700 hPa and b) 300 hPa for selected sites. The UKCA modelled concentrations are averaged from a 5-year model run. The observations are from an analysis by Logan (1999).

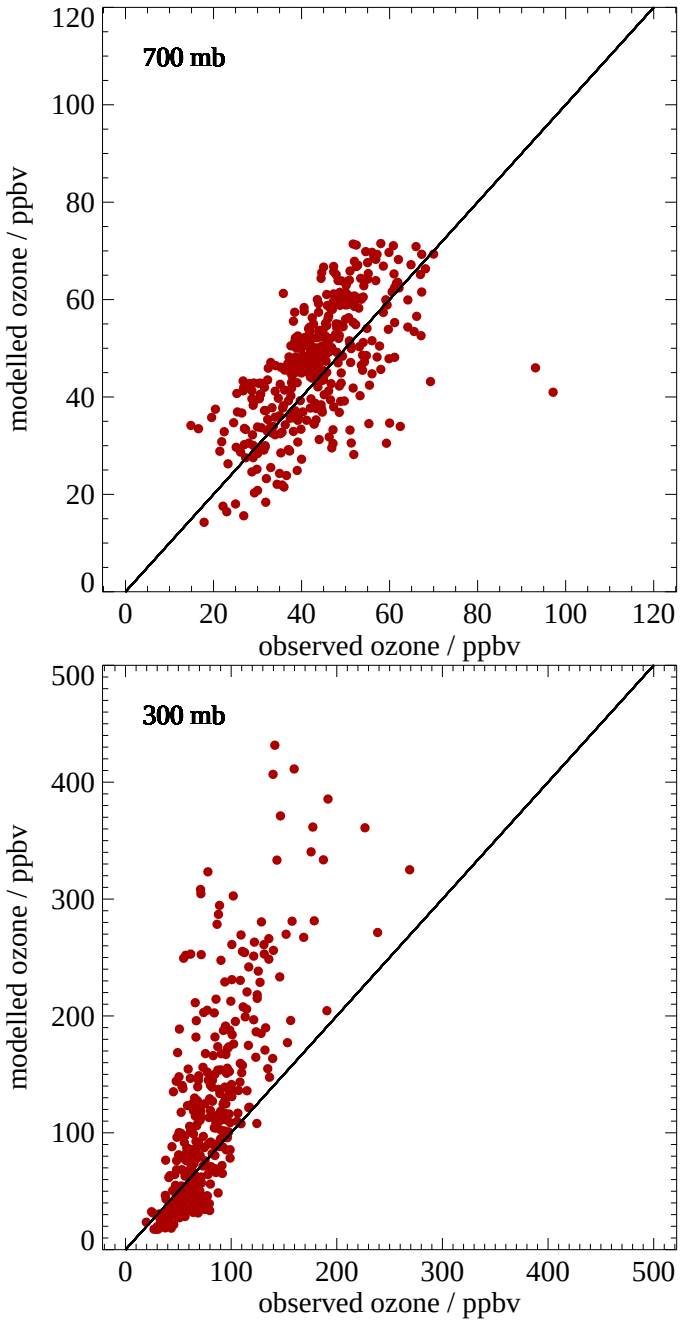

Figure 16: Scatter plot of modelled ozone concentrations against observed ozone concentrations at a) 700 hPa and b) 300 hPa. The UKCA modelled concentrations are averaged from a 5-year model run. The observations are from all sites in the Logan (1999) climatology.

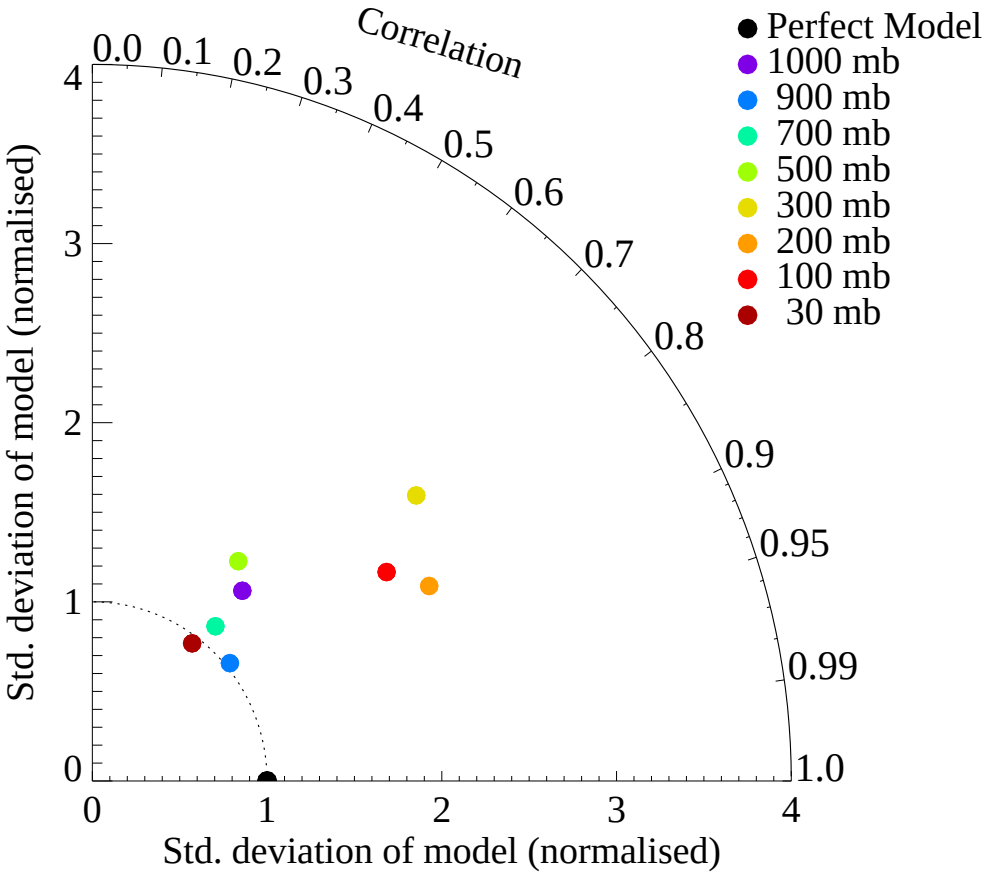

Figure 17: Taylor Diagram indicating the performance of UKCA modelled ozone concentrations at different pressure levels against climatological observations from Logan (1999). The 'perfect model' is represented in black.